JOURNAL OF MATERIALS SCIENCE 22 (1987) 2918–2926

Discontinuous precipitation in a dilute Co–3% Ti–2% Nb ternary alloy

J. OGENDER SINGH
University of Illinois at Urbana-Champaign, Department of Mechanical and Industrial Engineering, 1206 West Green Street, Urbana, Illinois 61801, USA

G. R. PURDY
Department of Metallurgy and Material Science, McMaster University, Hamilton, Ontario, Canada

Optical and electron microscopy have been used to follow the process of discontinuous precipitation in Co–3 wt % Ti–2 wt % Nb alloy. The initiation and growth of the discontinuous reactions occur in competition with well-advanced general coherent precipitation processes. The discontinuous reaction is close to equilibrium and is considered to be driven by the difference between coherent and incoherent equilibria in these systems. Analysis of velocity and spacing data indicate that the rates of the reactions are determined by grain boundary diffusion.

1. Introduction

Discontinuous precipitation is found in many alloy systems. Gust [1] and Williams and Butler [2] have presented an excellent and comprehensive review on the occurrence of discontinuous precipitation in binary and ternary systems. In brief, in certain alloy systems such as Pb–Sn, [3] Al–Ag [4] and Al–Zn [5] the movement of the other reaction front appears to be controlled by grain boundary diffusion. In other systems such as Co–Ta [6] and Ni–Ti [7], the motion of the reaction front is evidently controlled by the volume diffusion. There are many other systems such as Fe–Be [8] and Fe–W [9] in which both grain boundary and volume diffusion each play a role.

Very few investigations have been carried out on the occurrence of discontinuous precipitation in Co–Ti alloys. Fountain and Forgeng [10] and Blaise, *et al.*, [11], have reported the existence of discontinuous precipitation in binary Co–5% Ti and Co–9% Ti alloys on ageing at 973 and 1183 K, respectively. Thompson [12] has plotted the upper limit of discontinuous precipitation in binary Co–Ti alloys. The occurrence of discontinuous precipitation has also been reported by Viatour *et al.* [13] in Co–9% Ti–10% Fe and Shilling and Soffa [14] in Co–12% Fe–6% Ti ternary alloys. However, neither the structure nor the kinetics of the discontinuous reaction have been studied by these investigators. There appear to have been no prior detailed investigations of the effect of a third element on the precipitation process. A limited study on the effect of minor addition of lanthanum, niobium and iron to the base Co–3% Ti alloy was reported [15]. The aim of the present work was, therefore, to perform a detailed study on the morphology of discontinuous precipitation in Co–33% Ti–2% Nb alloys to acquire information concerning growth rate and interlamellar spacing, then to use this information to draw inference concerning the rate determining process. The results of ternary alloy were compared with the binary Co–3% Ti alloy [15].

2. Experimental procedure

Co–3 wt % Ti–2 wt % Nb alloy was supplied by the Cobalt Information Center, Belgium. Specimens for the microstructural observation were prepared by hot forging followed by cold rolling and intermediate annealing at 1073 K. All samples were homogenized at

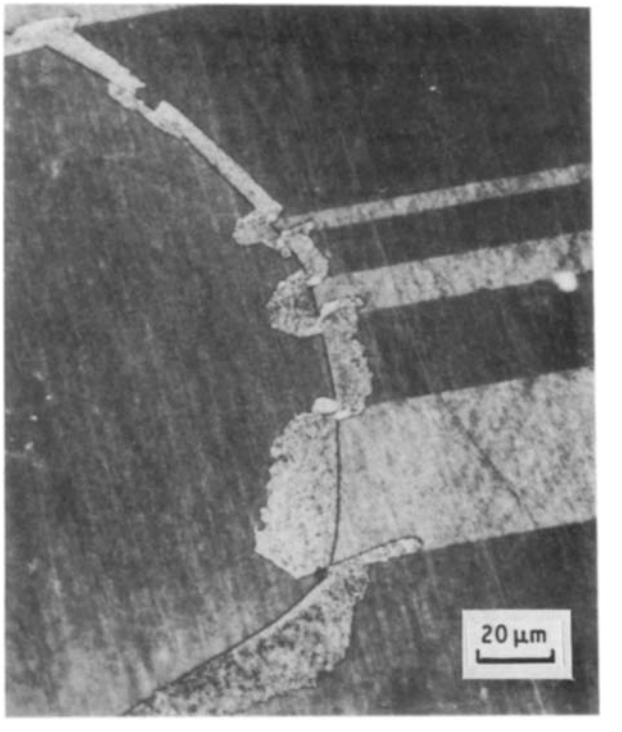

Figure 1 Optical micrograph of Co–3% Ti–2% Nb alloy aged at 873 K for 290 h showing effect of crystallographic orientation on the discontinuous precipitation.

0022–2461/87 $03.00 + .12

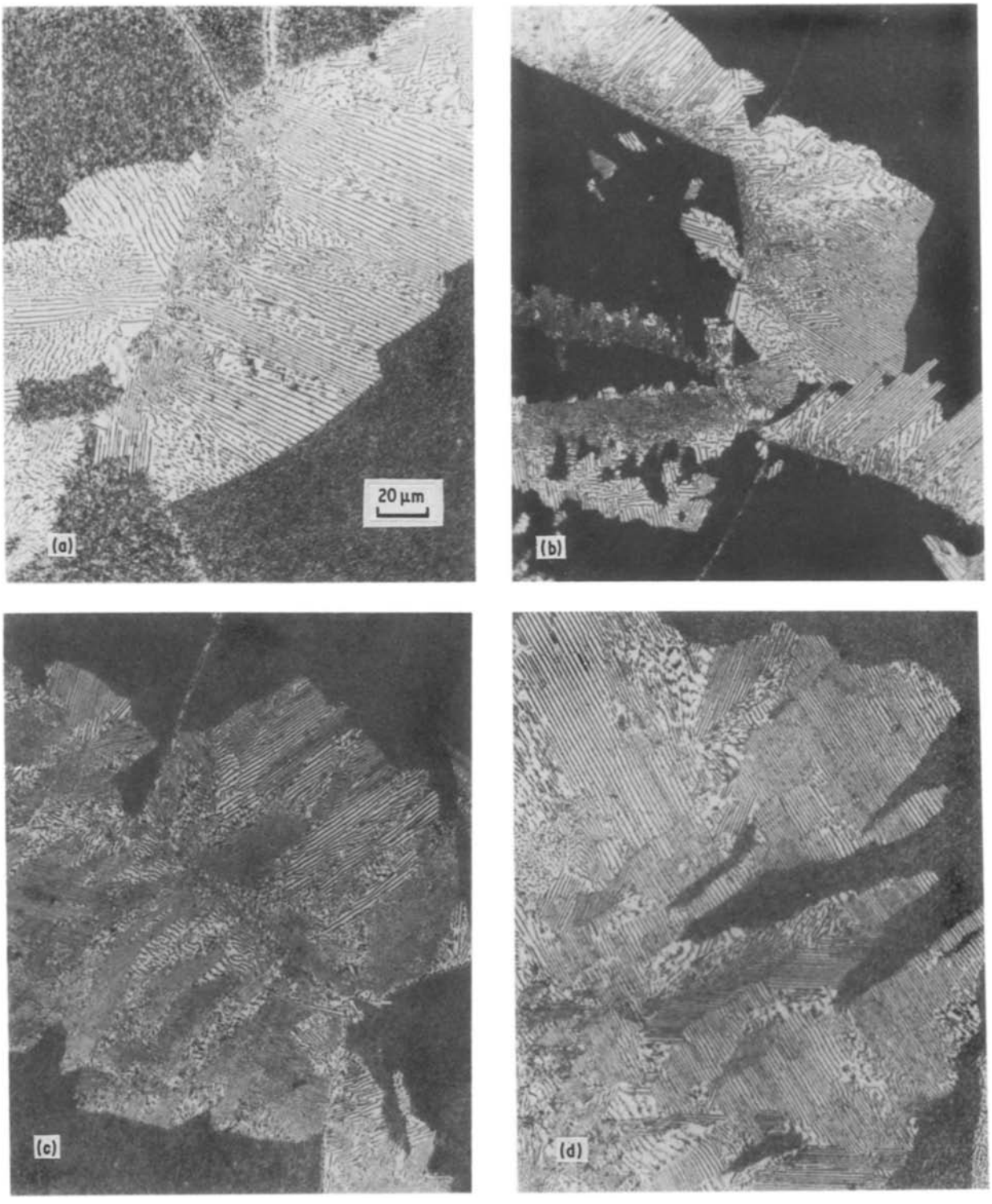

Figure 2 Optical micrograph of Co–3% Ti–2% Nb alloy aged at 1023 K for increasing times showing the development of discontinuous product with time (a) 120 h, (b) 240 h, (c) 350 h, and (d) 480 h.

1473 K for 1 h in evacuated sealed silica tubes and then quenched in water. Samples were aged at 823 to 1073 K. For optical metallography, 5% Nital was used as an etchant. Thin foils were prepared using a twin-jet polisher with a solution of 10% perchloric acid in methanol at 258 K. Foils were examined in transmission electron microscope, TEM (Phillips EM 300) and scanning transmission electron microscope, STEM (Vacuum Generator HB-5) at 100 kV.

3. Results

An optical micrograph of the Co–3% Ti–2% Nb alloy aged at 873 K for 290 h is shown in Fig. 1. The discontinuous precipitates were observed only at high angle boundaries (not at twins). The growth of the discontinuous product was found to be different at each side of the grain boundary and also within the twinned regions. Both lamellae and rods form within the product. The progressive development of discontinuous cells for different times at 1023 K is displayed in Fig. 2. The grain boundary reaction front is often severely faceted or cusped.

The early stage of growth of discontinuous precipitation in ternary alloy aged at 923 K for different times was investigated by TEM and is displayed in Fig. 3. Fig. 3a reveals high density and closely spaced

allotriomporphs at the grain boundary. The grain boundary is found to be almost straight. In addition, the presence of cuboid precipitates in the matrix is noted. The advanced growth of discontinuous cells is shown in Figs. 3b to 3f. Fig. 3c is a dark field electron micrograph taken with a matrix reflection to show the advancement of grain boundary. The radius of the rods was found to be about 80 nm (Fig. 3g). The lamellae were identified as Co_3Ti, an ordered phase. The dark field image from the superlattice reflection shows moiré fringes at the interface between the two phases. The spacing between the fringes was found to be approximately 9 nm (Fig. 3g). On ageing at a higher temperature (1073 K) for 360 h only grain boundary and general matrix precipitation were observed (Fig. 4). Moiré fringes were again observed at higher magnifications. (The fringe spacing in this case was approximately 4 nm).

The maximum displacements of the interface of discontinuous precipitation at different temperatures for ternary alloy is shown in Fig. 5. The growth rates as functions of temperature for Co–3% Ti and Co–3% Ti–2% Nb alloys are given in Fig. 6. The maximum migration rate of the discontinuous front in the binary and ternary alloys was found to occur at 923 and 973 K, respectively.

The interlamellar spacings were found by TEM and SEM as suggested by Gust, *et al.* [17]. No variation of measured spacing with time was detected. The reciprocals of interlamellar spacings for both the alloys with the function of ageing temperatures are shown in Fig. 7.

Microanalysis of samples were carried out in the STEM using quantitative X-ray spectroscopy. The analyses were performed in the stationary spot mode, thus permitting longer counting times and consequent reduced statistical uncertainty. For sufficiently thin foils, X-ray absorption can be neglected for characteristic X-ray with energies more than a few keV [18]. Then the characteristic X-ray intensities are functions of the foil thickness, but the X-ray intensity ratios for the several elements are independent of foil thickness. Ratios of X-ray characteristic maxima were converted to compositions based upon the Cliff–Lorimer [19]

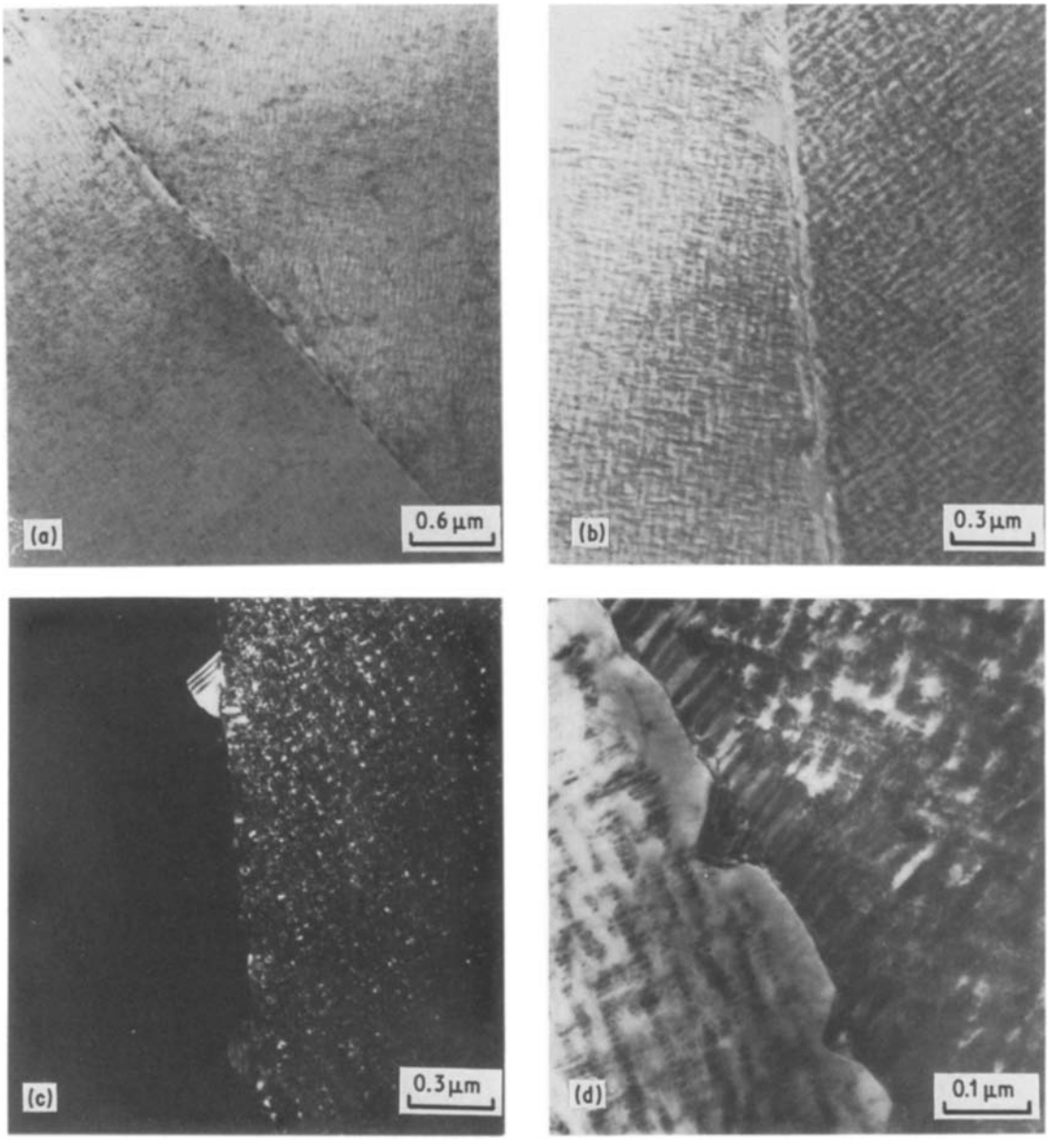

Figure 3 Transmission electron micrograph of Co–3% Ti–2% Nb alloys aged at 923 K for different times showing the growth of discontinuous cell (a) and (b) for 120 h; (c) and (d) for 240 h; and (f) and (g) 360 h.

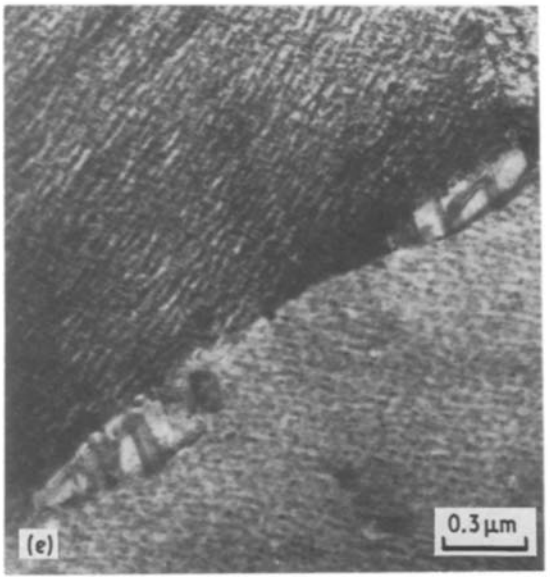

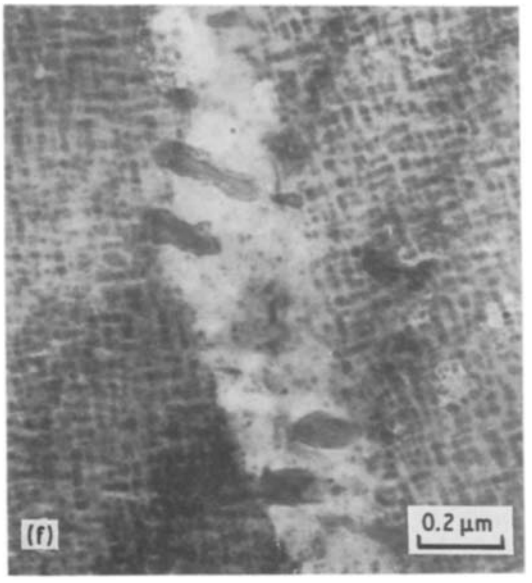

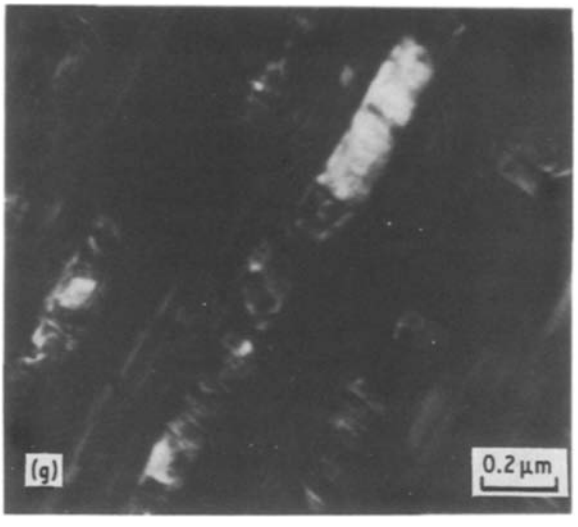

Figure 3 Continued.

approximation:

$$C_A/C_B = K_{AB} \quad I_A/I_B \tag{1}$$

$$C_C/C_B = K_{CB} \quad I_C/I_B \tag{2}$$

$$C_A + C_B + C = 1 \tag{3}$$

The concentration profile of the solutes titanium and niobium between the discontinuous lamellae is shown in Fig. 8.

4. Discussion

4.1. Initiation of discontinuous precipitation

From these results it is clear that the ternary Co–3 wt % Ti–2 wt % Nb alloy undergoes both general and discontinuous precipitation on ageing at temperatures below 973 and 1073 K, respectively. The initial stages of general decomposition in these alloys are rapid and may possibly involve spinoidal decomposition especially for deep quenches [20]. On ageing for longer periods, discontinuous precipitation is observed most frequently to start at high angle boundaries (Figs 1 to 3). The initiation of discontinuous precipitation thus involves the copious grain boundary precipitation in the form of globular incoherent or semi-coherent allotriomorphs of a stable precipitate. Only when these precipitates have coarsened can sections of the grain boundary be released and the celluar front develop.

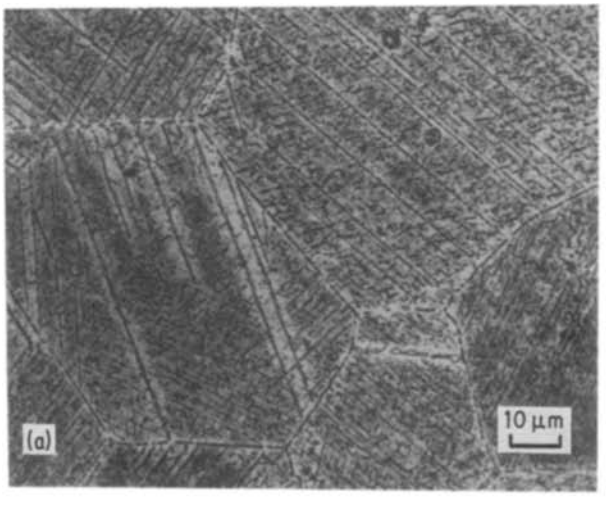

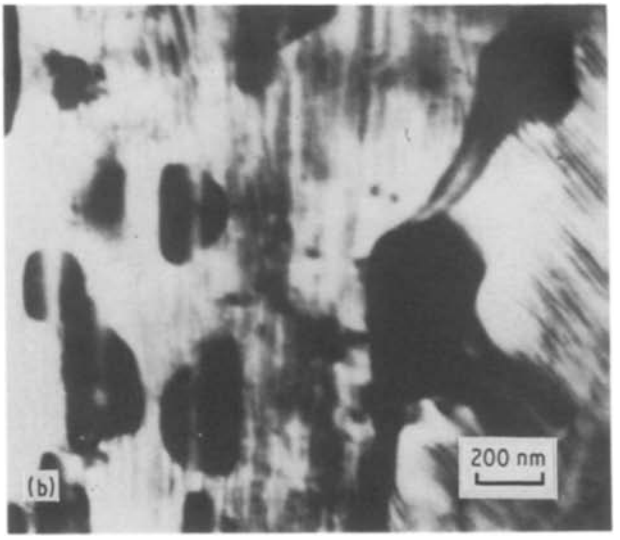

Figure 4 Optical micrograph of Co–3% Ti–32% Nb alloy aged at 1073 K for 360 h showing the grain boundary and matrix precipitation. (b) Transmission electron microscopy of the same aged alloy for one day showing disc and grain boundary precipitation.

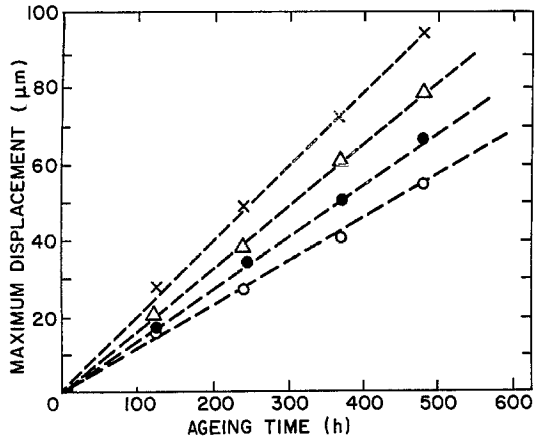

Figure 5 Plot of maximum displacement of the interface against time for Co–3% Ti–2% Nb alloys aged at various temperatures (○) 873 K, (△) 923 K, (x) 973 K, (●) 1023 K.

We note that the intragranular precipitates possessing coherency strain fields are less stable than the grain boundary allotriomorphs; a chemical potential difference thus exists for the migration of the solute atoms from the nearby cuboid precipitates to the grain boundary allotriomorphs, once coarsening conditions are established. As the grain boundary precipitates coarsen by competition among themselves and by competition with neighboring intergranular precipitates, the boundary regions between them will become enlarged. Thus, the coarsening process required to "unpin" boundary segments will probably take place very close to equilibrium and in the absence of significant local matrix supersaturation.

Previously proposed mechanisms for initiation of discontinuous precipitation fall into two broad classes: precipitate induced [21–23] and free boundary [24, 25]. Clearly, we are dealing here with the first type. Of the proposed mechanism for precipitate-induced migration, we can distinguish between those when a precipitate reaction acts to displace the boundary so as to reduce the interfacial free energy [21, 23] and those in which grain boundary diffusion of solute to precipitates sets up a chemical force for boundary migration against capillary forces [26].

For the present case, where we have argued that the matrix near the grain boundary must closely approach

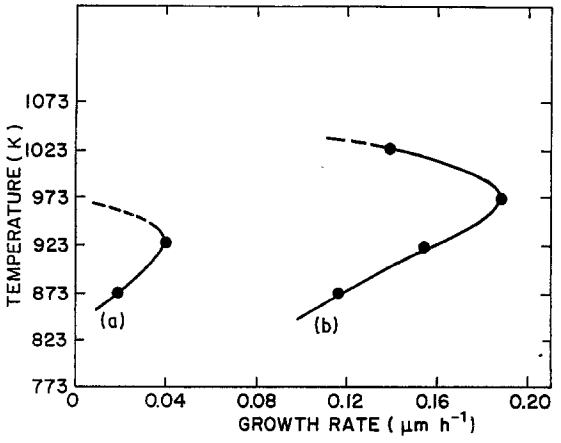

Figure 6 A plot of growth rate against time for (a) Co–3% Ti and (b) Co–3% Ti–2% Nb alloys.

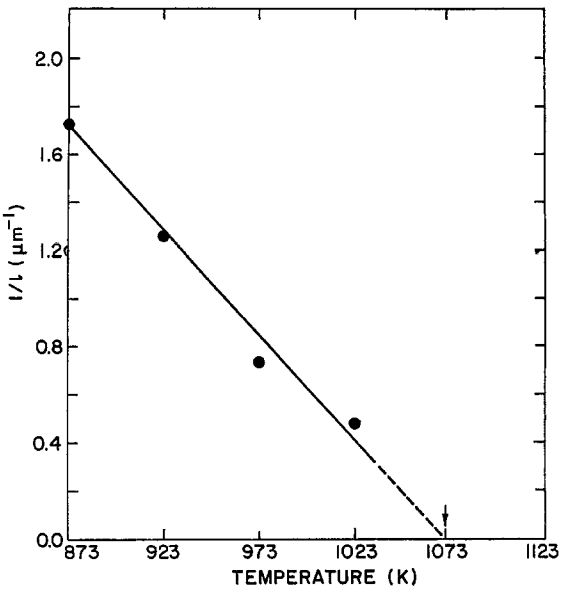

Figure 7 A plot of reciprocal interlamellar spacing against temperature for Co–3% Ti–2% Nb alloy. Extrapolating shows the upper temperature limit for discontinuous precipitation.

the incoherent equilibrium solute content at the time of initiation, we are inclined to favour an initiation mechanism involving a precipitate traction perhaps of the type proposed by Lange and Purdy [23] in which the initial displacement occurs when a segment of boundary pulls away from a shrinking precipitate (Fig. 9).

4.2. Growth of the discontinuous reaction products

The several methods of observation employed in this study each contribute to an overall view of the transformation. For the quantitative optical metallographic studies, we note the regular behaviour of the maximum velocity is a function of reaction temperature

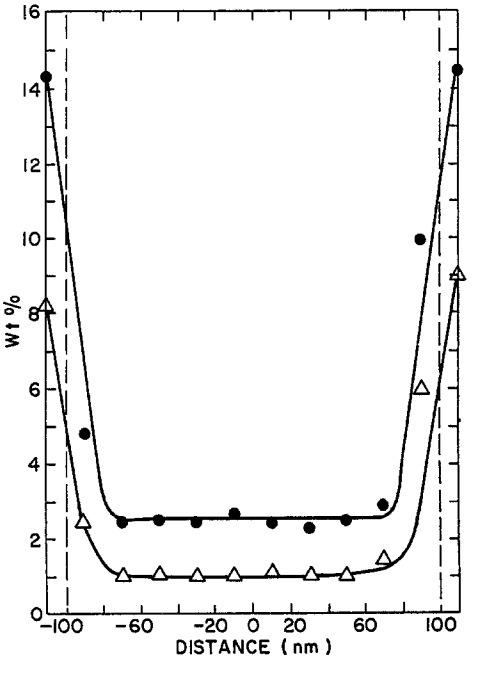

Figure 8 Composition profile between the lamellae in the discontinuous product in Co–3% ti–2% Nb alloy aged at 973 K. (●) Ti, (△) Nb.

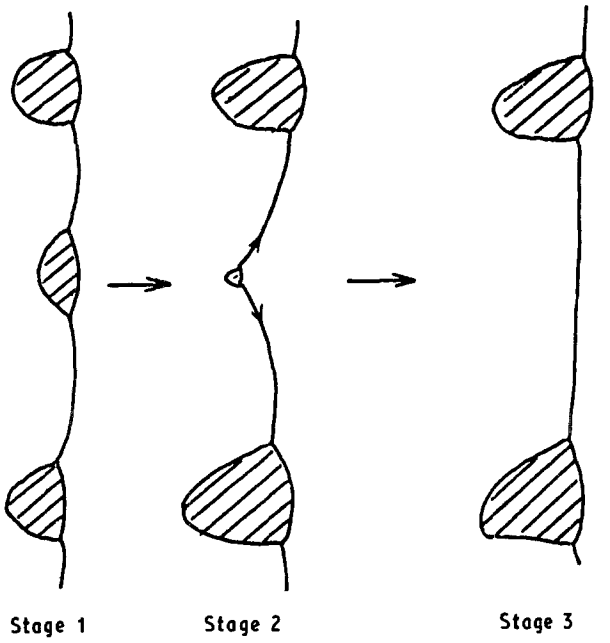

Figure 9 Three stages in a possible ageing sequence. In state 2, the equal size precipitate of state 1 has coarsened such that the other precipitates have grown carrying the grain boundary forward within them. When the boundary is released from the center (shrinking) precipitate it will straighten abruptly. After Lange and Purdy [16].

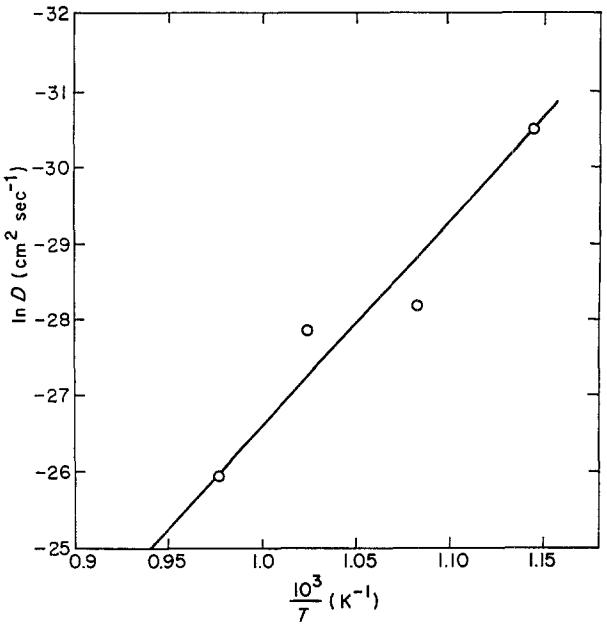

Figure 10 Plot of ln D against reciprocal temperature of Co–3% Ti–2% Nb alloys for determining the activation energy for the growth of discontinuous product.

(Fig. 6), the time-dependence of both maximum velocity and spacing at a given temperature and the self-consistent extrapolations (Fig. 7) of the upper limiting temperature for discontinuous precipitation in the alloy. However, a study of the optical micrographs reminds us that, by focusing on maximum displacements, we may lose sight of the major effects of anisotropy on migration, as reflected in the irregular cusped or faceted morphologies of the transformation front. We consider that the development of these facets is a direct consequence of the structure sensitivity of boundary migration, and would argue that this pronounced structure-sensitivity is closely related to the small driving force under which the front propagates. This is discussed more fully in the next sections.

The electron micrographs, on the other hand, draw attention to the completing reactions, involving the general precipitation and coarsening of coherent Co_3Ti type intermetallic compounds. For the times and temperatures under study, these competing transformations are well advanced; it is probable that the parent phase mixture seen by the discontinuous transformation front is very close to the full coherent equilibrium, as modified slightly by capillarity between Co_3Ti cuboids or Co_3 (Ti, Nb) discs and depleted cobalt rich solid solution.

The precipitate rods or plates in the discontinuous product have evidently lost full coherency (Fig. 3). Thus the main driving force for discontinuous precipitation is the difference between coherent and incoherent free energies of the two phase mixtures. This contention is consistent with the observations that discontinuous precipitation is absent in alloys where the general precipitates are incoherent or semi-coherent (Fig. 4) and that the maximum velocity and the spacing are constant with time for a given alloy and reaction temperature. Again, these observations and arguments place the transformation firmly in the "low driving force" category.

Microstructural (Fig. 3) and microchemical (Fig. 8) studies of the quenched transformation interface and its environs demonstrate that:

(a) The local interfacial curvature between Co_3Ti precipitates is uniform and small;

(b) The interface tends to bow slightly towards the parent phase matrix;

(c) The concentration profile is the depleted α-phase immediately behind the transformation which is essentially flat.

These observations, taken together, provide a strong indication that the local driving force is essentially uniform along the grain boundary segments between discontinuously formed plates or rods. This supports the recent findings in Al–Zn [5] and Mg–Al [27] alloys, and is consistent with the high-temperature behaviour of dilute Cu–Co alloys [28] where coherent rods form discontinuously from the matrix of coherent cobalt spheres in a deleted copper-rich matrix.

4.3. Cell growth kinetics

In order to determine the rate controlling factor in the reaction growth, it would be an ideal to study the change in solute composition across the advancing interface. Volume diffusion control reaction of Zener's type should result in a classical diffusion profile into the super saturated solid solution (as presented in Fig. 21a of [2]) while boundary controlled reaction would result in a discontinuous change in composition profile across the interface (as presented in Fig. 21b of [2]). There were competitive reactions involving the general fine and uniform homogeneous precipitation (i.e. spinoidal decomposition) and

TABLE I Growth and diffusion data for binary and ternary alloys

Temperature (K)	G(m sec^{-1}) Co–Ta [33]	G(m sec^{-1}) Co–Mg [34]	G(m sec^{-1}) Co–Ti–Nb	D^{V} (m^2 sec^{-1}) Co–Ta [33]	D^{V} (m^2 sec^{-1}) Cr–Co [34]	D^{V} (m^2 sec^{-1}) Co–Co [33]	D_V^Z (m^2 sec^{-1}) Equation 1	D_V^{MZ} (m^2 sec^{-1}) Equation 2	D_b^T (m^2 sec^{-1}) Equation 3	D_b^{MT} (m^2 sec^{-1}) Equation 4
873	–	–	0.33×10^{-10}	–	–	–	0.15×10^{-16}	0.20×10^{-16}	0.17×10^{-15}	0.55×10^{-16}
923	1.1×10^{-10}	0.5×10^{-8}	0.43×10^{-10}	7.0×10^{-20}	4.0×10^{-20}	8.0×10^{-21}	0.34×10^{-16}	0.35×10^{-16}	0.53×10^{-15}	0.13×10^{-15}
973	4.2×10^{-10}	0.8×10^{-7}	0.52×10^{-10}	3.4×10^{19}	2.5×10^{-19}	5.0×10^{-16}	0.88×10^{-16}	0.61×10^{-16}	0.24×10^{-14}	0.47×10^{-15}
1023	4.1×10^{-9}	0.2×10^{-7}	0.38×10^{-10}	3.5×10^{-18}	5.0×10^{-18}	2.5×10^{-19}	0.13×10^{-15}	0.54×10^{-16}	0.56×10^{14}	0.84×10^{-15}
1073	9.1×10^{-9}	0.8×10^{-7}	–	9.5×10^{-18}	2.0×10^{-18}	1.0×10^{-18}	–	–	–	–

TABLE II Comparison of activation energies and D_0 values

	Q (KJ mol^{-1}) Co–Co [35]	Q (KJ mol^{-1}) Co–Ti–Fe	Q (KJ mol^{-1}) Cu–Mg [34]	Q (KJ mol^{-1}) Co–Ti–Nb				D_0^{Co-Co} (m^2 s^{-1})	
								Ref [35]	Calculated
Volume (V)	243	331 [36]	234	319 [15]				3.0×10^{-7}	Equation 1: 0.94×10^{-10} Equation 2: 0.39×10^{-13}
				Equation 1	Equation 2	Equation 3	Equation 4		
Boundary (b)	117	234 [16]	139	113	54	178	140	1.2×10^{-7}	Equation 3: 0.75×10^{-5}
$\frac{Q_b}{Q_v}$	0.48	0.7	0.6	0.35	0.17	0.56	0.44		Equation 4: 0.14×10^{-7}

coarsening of coherent Co_3Ti type intermetallic compounds in the matrix and a head of the interface of discontinuous precipitation. In such cases, it is very difficult to measure the composition profile ahead of interface as discussed above. In such cases, various models for the cell growth would be tested using the experimental data and they are discussed as follows.

The cell growth rate (G) is given by Zener's equation, when the cell growth is controlled by volume diffusion mechanism [29]

$$G = 2\frac{(X_0 - X_e)}{X_0}\frac{D_v^Z}{l} \quad (4)$$

where D_v^Z is the volume diffusion coefficient of solute atoms titanium in cobalt matrix, X_0 and X_e are the initial solute concentration and equilibrium concentration of depleted matrix, respectively, and l is the interlamellae spacing. Equation 4 could be employed only for the alloys undergoing discontinuous precipitation. In addition to discontinuous precipitation, continuous precipitation also occurred in the matrix of this ternary alloy; therefore, Zener's modified equation proposed by Aaronson and Clark [4] should be tested and is given by

$$G = \frac{(X_m - X_e)}{(X_\beta - X_0)}\frac{(X_\beta - X_e)}{(X_0 - X_e)}\frac{2D_v^{MZ}}{l} \quad (5)$$

where X_m is the matrix composition ahead of the interface. X_β is the composition of second phase $Co_3(Ti, Nb)$. The activation energy (Q_v^{MZ}) and D_0 calculated by Equation 5 is 54 KJ mol^{-1} and 0.387 $\times$ 10^{-13} m^2 sec^{-1}, respectively. The estimated D_0^v value is higher than the volume self-diffusion of pure cobalt (Tables I and II). Therefore the cell growth rate cannot be represented by Equations 4 and 5.

Turnbull proposed the following growth equation when cell growth is controlled by grain boundary diffusion mechanism [30].

$$G = \frac{2(X_0 - X_e)}{X_0}\frac{\lambda D_b^T}{l^2} \quad (6)$$

where D_b is the grain boundary diffusion coefficient and λ is the effective boundary thickness (≈ 50 nm). Aaronson and Liu [31] modified Turnbull's equation as follows:

$$G = 4\lambda D_b^{MT}/l^2 \quad (7)$$

D_v, D_b, D_0, and activation energy values obtained from Equations 4 to 7 are presented in Tables I and II. The experimentally found values for the present alloy are compared with those for other binary alloys. Unfortunately, diffusion data are not available for these materials and a more detailed analysis is therefore precluded.

D_0 estimated from Equation 6 is higher than the grain boundary diffusion for pure cobalt. Therefore, Equation 7 seems the more reasonable to express the cell growth in this alloy. From the above consideration, it can be concluded that the cell growth is controlled by the grain boundary diffusion.

5. Conclusions

We have examined the discontinuous precipitation processes in Co–Ti–Nb alloy. The processes are slow; their occurrence and rates are extremely structure-sensitive and we find that there exists everywhere a competition between incoherent discontinuous precipitation and advanced coherent general precipitation. It is, therefore, inferred that the reactants and products for the discontinuous precipitation forces are each close to equilibrium and that the growth (and to some extent the initiation) of the discontinuous product is determined primarily by differences between coherent and incoherent equilibria. Analysis of the experimental (maximum) rate and spacing data on the basis of grain boundary diffusion controlled growth gives reasonable accord with published diffusion data.

Acknowledgements

This research was supported by the National Science and Engineering Research Council, Canada. Discussions with J. S. Kirkaldy and I. G. Solorzano are gratefully acknowledged.

References

1. W. GUST in "Phase Transformations", Vol. 1 (The Institution of Metallurgists, London, 1979) p. 27.
2. D. B. WILLIAMS and E. P. BUTLER, *Int. Met. Rev.* **26** (1981) 153.
3. Y. C. LIU and H. I. AARONSON, *Scripta Met.* **2** (1968) 1.
4. H. I. AARONSON and J. B. CLARK, *Acta Met.* **16** (1968) 845.
5. I. G. SOLORZANO and G. R. PURDY, *Met. Trans.* **15A** (1984) 1055.
6. M. KORCHYNSKY and R. W. FOUNTAIN, *Trans. AIME* **215** (1959) 1033.
7. J. R. MILHALISIN and R. F. DECKER, *Trans. Met Soc. AIME* **218** (1960) 507.
8. J. HIGGINS, R. B. NICHOLSON, AND P. WILKES, *Acta Met.* **22** (1974) 201.
9. HORNBOGE, *Z. Metallk.* **52** (1961) 47.
10. R. W. FOUNTAIN and W. D. FORGENG, *Trans. AIME* **215** (1959) 998.
11. J. B. BLAISE, P. VIATOUR and J. M. DRAPIER, *Cobalt* **49** (1970) 192.
12. M. N. THOMPSON, PhD Thesis, Cambridge University, Cambridge, UK (1971).
13. P. VIATOUR, J. M. DRAPIER and D. COUTSOURADIS, *Cobalt* **3** (1973) 67.
14. J. W. SHILLING and W. A. SOFFA, *Acta Met.* **26** (1978) 413.
15. J. SINGH, S. LELE and S. RANGANATHAN in Proceedings of International Conference on Solid–Solid Phase Transformation, Carnegie Mellon University, Pittsburgh, USA (1981) p. 975.
16. J. SINGH, S. LELE and S. RANGANATHAN, *Z. Metallk.* **72** (1981) 467.
17. W. GUST, B. PREDEL and U. ROLL, *ibid.* **6B** (1977) 117.
18. R. W. CARPENTER, J. BENTLEY and E. A. KENIK in Proceedings of Workshop on Analytical Electron Microscopy, IIT Research Institute, Chicago, Illinois, Vol. 1 (1977) p. 411.
19. G. CLIFF and G. W. LORIMER in Proceedings of the 5th European Congress on Electron Microscopy, Manchester, Institute of Physics (London, 1972) p. 140.
20. J. SINGH, S. LELE and S. RANGANATHAN, *J. Mater. Sci. and Engng.* (in press).
21. K. N. TU and D. TURNBULL, *Acta Met.* **15** (1967) 369.
22. H. I. AARONSON and H. B. AARON, *Met. Trans.* **3** (1972) 2743.
23. N. LANGE and G. R. PURDY in Report of the Royal Institute of Technology, Stockholm (1067).

24. R. A. FOURNELLE and J. B. CLARKE, *Met. Trans.* **3** (1971) 2757.
25. G. MEYRICK, *Scripta Met.* **10** (1976) 649.
26. I. G. SOLORZANO, G. R. PURDY and G. WEATHERLY, *Acta Met.* **32** (1984) 1709.
27. D. A. PORTER and EDDINGTON, *Proc. R. Soc.* **358A** (1977) 335.
28. A. PEROVIC and G. R. PURDY, *Acta Met.* **29** (1982) 53.
29. C. ZENER, *Trans. AIME* **167** (1946) 550.
30. D. TURNBULL, *Acta Met.* **3** (1955) 55.
31. H. I. AARONSON and Y. C. LIU, *Scripta Met.* **2** (1968) 1.
32. J. W. CAHN, *Acta Met.* **1** (1959) 18.
33. M. KORCHYNSKY and R. W. FOUNTAIN, *Trans. Met Soc. AIME* **215** (1959) 1033.
34. H. TSUKAKINO and R. NOZATO, *J. Mater. Sci.* **19** (1984) 3013.
35. F. H. WOHLBIER (ed.) in "Diffusion and Defects Data", Vol. 12, (1976) p. 34.
36. J. SINGH, S. LELE and S. RANGANATHAN, *J. Mater. Sci.* **15** (1980) 2010.

Received 30 September
and accepted 15 December 1986